Optimization of Hierarchical Sliding Mode Control Parameters for a Two-Wheeled Balancing Mobile Robot Using the Firefly Algorithm

Ngoc-Linh Tao [1], Dinh-Hieu Pham [2], Minh-Khoi Pham [3], Thi-Van-Anh Nguyen [4*]
[1] School of Mechanical Engineering, Hanoi University of Science and Technology, Hanoi, Vietnam
[2,3,4] School of Electrical and Electronic Engineering, Hanoi University of Science and Technology, Hanoi, Vietnam
Email: [1] linh.taongoc@hust.edu.vn, [2] hieu.pd202625@sis.hust.edu.vn,
[3] khoi.pm202425@sis.hust.edu.vn, [4] anh.nguyenthivan1@hust.edu.vn
*Corresponding Author

***Abstract*—Two-wheeled balancing Mobile Robots (2WBMRs) are inherently unstable, posing significant challenges in control. This paper addresses the problem of optimizing control parameters for such systems to improve stability and overall performance. The proposed solution integrates Hierarchical Sliding Mode Control (HSMC) with the Firefly Algorithm, which is a stochastic algorithm inspired by the flashing behavior of fireflies, to optimize control performance. The research contribution is the development of an optimized control system where the Firefly Algorithm is used to fine-tune HSMC parameters, ensuring improved stability and responsiveness. Additionally, the integration of Sliding Mode Control (SMC) within the HSMC framework provides precise yaw angle stabilization, contributing to comprehensive robot control. In this approach, the Firefly Algorithm is applied to optimize the HSMC parameters due to its capability to optimize multi-dimensional variables and its robust optimization abilities, aiming to enhance the stability of the vehicle in the best possible way. Simulations were conducted to compare the proposed method before and after applying the optimization algorithm, evaluating key performance metrics such as response time and stability. The results indicate a (10%) improvement in stability, demonstrating that the Firefly Algorithm significantly enhances control performance. These findings suggest that the optimized control system not only improves the stability of 2WBMRs but also has potential applications in broader dynamic control systems. In conclusion, based on the research results, we can conclude that the use of the HSMC-SMC controller for nonlinear systems like 2WBMRs is feasible and can be applied to many other nonlinear systems. Furthermore, the Firefly Algorithm has proven to be a powerful tool for optimizing parameters in control systems and can be applied in robotics and automation systems.**

Keywords*—Two-Wheeled Balancing Mobile Robots; Hierarchical Sliding Mode Control; Sliding Mode Control; Stability Control; Firefly Algorithm; Parameters Optimization

I. INTRODUCTION

In this day and age, the rapid advancements in robotics science and technology have been transforming industries and enhancing everyday life, with applications spanning various fields, including manufacturing, transportation, logistics, healthcare, and scientific research [1]–[8]. Notable examples include automated assembly lines and surgical-assisting robots. As such, the potential of robotic systems to revolutionize processes across sectors is inevitable. Among these innovations, mobile robots have demonstrated tremendous promise in various fields, offering flexibility, efficiency, and numerous practical applications in daily life. In particular, wheeled robots have become an indispensable part of industrial automation and transportation due to their inherent mobility. For instance, four-wheeled robots [9], [10] can operate stably and move rapidly on flat surfaces and are widely applied in autonomous robotic vehicle (ARV) systems, yet they struggle in narrow or inclined environments. Hence, a balancing system becomes crucial in such scenarios. Two-Wheeled Balancing Mobile Robots (2WBMR) offer an optimal and promising solution to overcome the limitations of traditional four-wheeled vehicles. Based on their flexibility, they have been widely applied in real-world scenarios, such as personal transportation (e.g., Segway), or as support robots in rescue operations and research. Additionally, they can be developed for use in light industrial transportation. With its structure comprises three main bodies: the right wheel, the left wheel, and an inverted pendulum. the two wheels, located on either side of the robot, provide the primary means of movement and balance, The inverted pendulum, mounted vertically between the wheels, represents the main challenge in the system's control design. This pendulum acts as an inherently unstable body, requiring constant feedback and corrective forces from the wheels to maintain an upright position. Due to its two-wheel design, it allows for more flexible movement and the ability to maintain an upright posture on inclined surfaces. This is an intriguingly stable system, capable of performing three degrees of freedom motion, including tilt, lateral movement, and forward movement with just two wheels [11]–[14]. Especially, based on the differential system between its two wheels, 2WBMR can maneuver flexibly, rotating in any direction. This differential system is also implemented in trains to ensure safety and stability. When the train moves off course, the right wheel spins faster or slower than the left, causing the train to veer either to the left or the right. Despite its many advantages in mobility, 2WBMRs are inherently unstable systems, highly sensitive to external factors such as sudden movements, uneven terrain, external disturbances, or obstacles in their operating environment. Even minor changes in the load's weight can lead to system instability. A control system is required to manage the robot in real-time to maintain balance. In practical applications, such as industrial environments with moving obstacles or unpredictable conditions, the demand for fast response times and high stability becomes even more critical to ensure the robot's reliable performance. Therefore, the control of a two-wheeled balancing robot is a challenging task due to its inherently unstable nature, requiring precise and adaptive control strategies to maintain equilibrium [15]–[18].

Over the years, various control methods have been explored to address the challenges posed by real-world robotic systems. Classical methods, such as the Proportional-Integral-Derivative (PID) [19]–[21] controller and Linear Quadratic Regulator (LQR) [22], [23], have been widely employed due to their simplicity and effectiveness in linear systems. However, these methods are limited in handling nonlinear systems, such as the 2WBMR system, especially in complex environments where the system is subject to significant disturbances or rapid changes. For instance, PID controllers often struggle with maintaining stable states and exhibit slow response times in highly dynamic systems. Meanwhile, the LQR optimizes system performance by minimizing the cost function, proving effective in achieving stability and precise dynamic control [24]. Nevertheless, the LQR controller is constrained by its reliance on the system model, making it less efficient when dealing with nonlinear models or external disturbances. The combined with PID control, LQR offers a straightforward adjustment mechanism but face limitations in handling nonlinear systems or strong disturbances [25]–[28]. Control methods such as Sliding Mode Control (SMC) have been developed to overcome these limitations by offering greater robustness and adaptability, making them suitable for the 2WBMR system. [29], [30] SMC is favored for its resilience against external disturbances, its ability to handle nonlinear models, its insensitivity to parameter variations, independence from peripheral reactions, fast response, and ease of implementation [31]–[35]. Several SMC methods have been proposed and implemented, including Adaptive SMC [36]–[38], Terminal SMC [39], [40], and Hierarchical Sliding Mode Control [41], [42]. While this control approach provides many advantages, it has a drawback in the form of inherent chattering. Similarly, Active Disturbance Rejection Control (ADRC) [43], [44] utilizing an Extended State Observer (ESO) to estimate and compensate for disturbances and unmodeled dynamics such as friction and wear [45]. This method offers a flexible and robust solution for maintaining stability in uncertain and noisy conditions. However, it faces challenges in the extremely complex process of parameter tuning. Each of these control methods—SMC, ADRC, LQR, and PID [46], [47] contributes to improving the performance and stability of 2WBMR systems, with each approach suited to different operational challenges and requirements. However, every technique also comes with its own distinct advantages and disadvantages.

An extended approach to SMC is Hierarchical Sliding Mode Control (HSMC), which has garnered significant attention in the control of underactuated systems depending on the hierarchical structure sliding surfaces, each sliding surface represents a specific output variable of the system, the simplest is composed of error and derivative of it, and the control strategy operates to keep the system on these surfaces, adjusting the deviations to maintain stability [48]–[51]. Therefore, applications of HSMC include the control of double-pendulum crane systems [52], [53], two-wheeled self-balancing vehicles [54], [55], and the longitudinal movement of spherical robots [56], [57]. HSMC is particularly effective in Single Input Multiple Output (SIMO) systems, utilizing two types of sliding surfaces. The first-order sliding surface is defined for each state variable to determine the control signal that drives the system toward the sliding surface. The second-order sliding surface, which is a linear combination of the first-order sliding surfaces, provides the control signal that ensures the system remains on the sliding surface. The coordinated use of these two sliding surfaces enables efficient control of systems with multiple interacting states and control variables. Compared to other methods like PID and LQR, HSMC is particularly efficient in dealing with the nonlinearities, uncertainties inherent in unstable and underactuated systems, making it an ideal choice for such applications. In addition, since HSMC is an advanced technique of the SMC method, it will still experience Chattering [58]–[60], which is a high-frequency oscillation that occurs when the control signal changes too rapidly near the sliding surface, causing undesirable vibrations in the system. However, this can be mitigated by selecting appropriate control parameters.

Building on the HSMC previously introduced to stabilize the body of the 2WBMR, the integration of an SMC for yaw angle control provides a crucial enhancement. This addition ensures a more comprehensive control model, significantly improving overall system performance. Previous studies have largely overlooked the yaw angle [24], [45]thereby preventing the system from being controlled in a fully comprehensive manner.

Although the design of HSMC and SMC controllers is not overly complex, they involve a large number of control parameters and lack a fixed tuning method, making the task of parameter adjustment difficult and time-consuming. Consequently, utilizing optimization algorithms to automatically identify optimal parameter values is essential and has been widely embraced by researchers. [61]–[65] The Firefly Algorithm (FA) [66]–[69] , in particular, demonstrates exceptional performance in optimizing systems that have multiple parameters. FA was proposed by Yang in 2008 and is a stochastic algorithm inspired by the flashing behavior of fireflies, which use their light to attract mates and ward off predators. This algorithm builds upon and advances previous algorithms like Particle Swarm Optimization (PSO) and Genetic Algorithm (GA) by incorporating both the capability to inherit and improve upon better solutions while maintaining randomness to avoid local optima. Due to these characteristics, the Firefly Algorithm has been applied to numerous control optimization problems., such as optimizing trajectory planning [70]–[72], tuning parameters for Fuzzy controllers [73]–[75] and other control systems [76], [77].

While previous research articles have disregarded the yaw angle and lacked optimization algorithms for the controller's performance, this has resulted in suboptimal system response times, and the absence of the yaw angle in the model can complicate control on real surfaces. By controlling both body stabilization and yaw orientation, the combined HSMC-SMC approach, along with the utilization of the optimization algorithm Firefly Algorithm, enables higher precision control, enhances stability, and improves response times. Furthermore, controlling the yaw angle increases the system's comprehensiveness, opening up new control strategies for the future, allowing for free movement on surfaces at will or according to specified terrain [78]–[80]. This represents a significant foundational step for further research when applying the system in real-world scenarios, such as industrial environments with substantial disturbances and undefined loads. Thus, the research has successfully achieved stable control and direction maneuvering of the 2WBMR to ensure comprehensive system control and potential real-world applications. Additionally, the study has applied the firefly algorithm, a powerful yet not widely used optimization technique, to optimize the system control parameters and enhance stability performance.

In this paper, we propose a Hierarchical Sliding Mode Control (HSMC) combined with Sliding Mode Control (SMC), optimized using the Firefly Algorithm to ensure stable control of a two-wheeled balancing mobile robot. The remainder of the paper is organized as follows: The Introduction discusses the background, the challenges of controlling two-wheeled balancing robots, and the need for optimization in control methods. The Method section describes the dynamic model of the robot and the design of the HSMC-SMC controller, along with the Firefly Algorithm used for optimization. In the Results and Discussion, we present the simulation results that assess both the stability of the HSMC-SMC controller and the optimization performance of the Firefly Algorithm. Finally, the Conclusion summarizes the key findings and suggests directions for future work.

II. METHOD

A. Two-Wheeled Balancing Mobile Robot Modeling

Fig. 1 depicts the Two-Wheeled Balancing Mobile Robot (2WBMR) system, illustrating its chassis with two independently actuated wheels and the control unit responsible for stability and maneuverability. The diagram presents three mutually independent frames: frame {N} with three unit axes (n_1, n_2, n_3), which is fixed and attached to the ground; frame {M} with three unit axes (m_1, m_2, m_3), attached at the midpoint of the wheel axis; and frame {B} with three unit axes (b_1, b_2, b_3), attached to the center of mass of the pendulum.

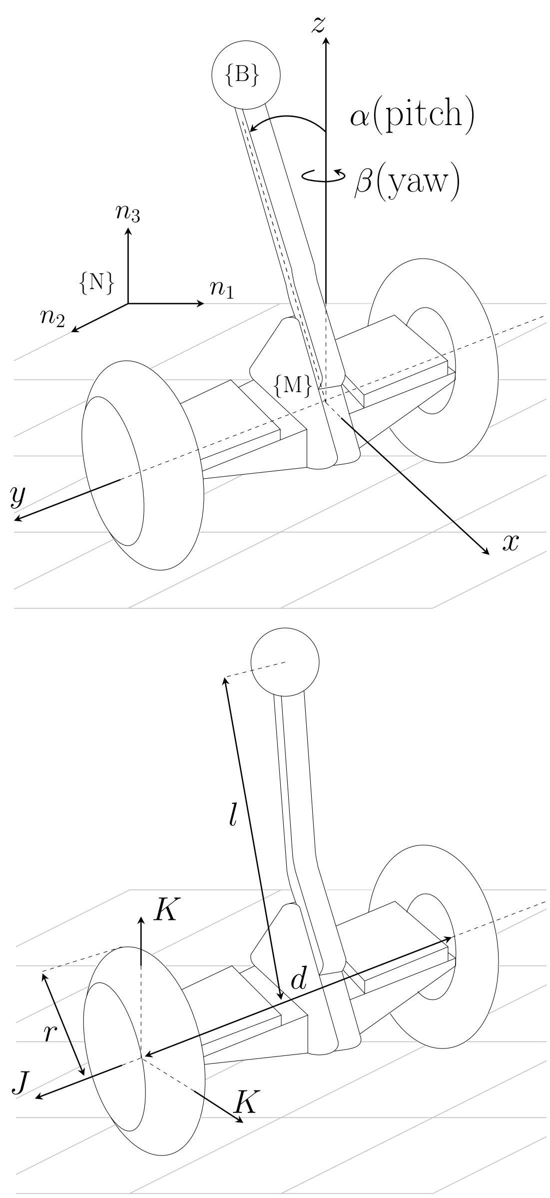

Fig. 1. Two-wheeled Balancing Mobile Robot

In the Fig. 1, d represents the distance between the two wheels, l is the length of the inverted pendulum of the 2WBMR, and r is the radius of the wheels. m_B and m_W are the masses of the pendulum (excluding the wheels) and each wheel, respectively. I_1, I_2, and I_3 denote the moments of inertia about the three coordinate axes of the inverted pendulum's center of mass. Additionally, J and K represent the moments of inertia about the vertical axis through the wheel and perpendicular to the corresponding axis, respectively.

Note that the subscripts below denote the position being considered, including the left and right wheels, the midpoint of the wheel axis, and the inverted pendulum, corresponding to L, R, C, and B, respectively. The superscripts on the upper indicate the frames (with frame N having no symbol). The information about the parameters of the two wheels (L, R) and the inverted pendulum body (B) are in Table I:

TABLE I. VARIABLES AND DEFINITIONS OF THE 2WBMR SYSTEM

Symbol	Definition
$\omega_L, \omega_R, \omega_B$	Angular velocity vectors of (L, R, B)
v_L, v_R, v_B	Velocity vectors of the center of mass of (L, R, B)
v_M, ω_M	Linear and angular velocity vector in the $\{M\}$ frame
x_C, y_C, z_C	Position of the center point of the system in the $\{M\}$ frame
T_L, T_R	Wheel torques at (L, R)
γ_L, γ_R	Rotation angles of (L, R)
$\dot{x}, \dot{\alpha}, \dot{\beta}$	Forward velocity, pitch rate, yaw rate
f_L, f_R	Damping torques at (L, R)

The center of mass of each body is governed by the holonomic constraints:

$$\begin{aligned} x_B &= x_C + l\sin\alpha\cos\beta, \\ x_L &= x_C - \frac{d}{2}\sin\beta, \\ x_R &= x_C + \frac{d}{2}\sin\beta, \quad y_B = y_C + l\sin\alpha\sin\beta, \\ y_L &= y_C + \frac{d}{2}\cos\beta, \quad y_R = y_C - \frac{d}{2}\cos\beta, \\ z_B &= l\cos\alpha. \end{aligned} \tag{1}$$

Assuming the model's motion lacks slipping, the longitudinal velocity of the wheels depends on the wheel radius and angular velocity. Additionally, the yaw angle is constrained based on the velocities of the left and right wheels. According to the paper in [11], there are nonholonomic constraints:

$$\begin{aligned} \dot{x}_L\cos\beta + \dot{y}_L\sin\beta &= r\dot{\gamma}_L, \\ \dot{x}_R\cos\beta + \dot{y}_R\sin\beta &= r\dot{\gamma}_R, \\ (\dot{x}_L + \dot{x}_R)\sin\beta &= (\dot{y}_L + \dot{y}_R)\cos\beta. \end{aligned} \tag{2}$$

which are equivalent to:

$$\begin{aligned} \dot{x}_C\cos\beta + \dot{y}_C\sin\beta - \frac{d}{2}\dot{\beta} - r\dot{\gamma}_L &= 0, \\ \dot{x}_C\cos\beta + \dot{y}_C\sin\beta - \frac{d}{2}\dot{\beta} - r\dot{\gamma}_R &= 0, \\ \dot{x}_C\sin\beta - \dot{y}_C\cos\beta &= 0. \end{aligned} \tag{3}$$

If we apply the relationships of the 7 holonomic constraints in 1 and the 3 nonholonomic constraints in 3, we can easily confirm that the 2WBMR system has 3 degrees of freedom of motion, including translation, rotation, and tilt.

By differentiating both sides of the equation (1), the velocities of the three parts {L,R,B} are determined corresponding to the {N} trajectory system. Thus, the following equations are obtained:

$$\begin{aligned} v_L &= (\dot{x}_C - \frac{d}{2}\dot{\beta}\cos\beta)n_1 + (\dot{y}_C - \frac{d}{2}\dot{\beta}\sin\beta)n_2, \\ v_R &= (\dot{x}_C + \frac{d}{2}\dot{\beta}\cos\beta)n_1 + (\dot{y}_C + \frac{d}{2}\dot{\beta}\sin\beta)n_2, \\ v_B &= (\dot{x}_C + l\dot{\alpha}\cos\alpha\cos\beta - l\dot{\beta}\sin\alpha\sin\beta)n_1 \\ &\quad + (\dot{y}_C + l\dot{\alpha}\cos\alpha\sin\beta + l\dot{\beta}\sin\alpha\cos\beta)n_2 \\ &\quad - (l\dot{\alpha}\sin\alpha)n_3. \end{aligned} \tag{4}$$

The angular velocities of the three bodies [11] are described by the following equations for rotational motion:

$$\begin{aligned} \omega_L &= \omega^M + \dot{\gamma}_L m_2 = \dot{\beta}m_3 + \left(\frac{1}{r}\right)(\dot{x} - \frac{d}{2}\dot{\beta})m_2, \\ \omega_R &= \omega^M + \dot{\gamma}_R m_2 = \dot{\beta}m_3 + \left(\frac{1}{r}\right)(\dot{x} + \frac{d}{2}\dot{\beta})m_2, \\ \omega_B &= \omega^M + \dot{\alpha}b_2 = (-\dot{\beta}\sin\alpha)b_1 + \dot{\alpha}b_2 + (\dot{\beta}\cos\alpha)b_3. \end{aligned} \tag{5}$$

To apply the Euler-Lagrange equation, it's necessary to compute the total kinetic and potential energy of the 2WBMR system. The expression for the translational kinetic energy of the 2WBMR can be formulated as:

$$T_{trans} = \frac{1}{2}m_W(v_L)^T.v_L + \frac{1}{2}m_W(v_R)^T.v_R + \frac{1}{2}m_B(v_B)^T.v_B \tag{6}$$

The rotational energy of the 2WBMR can be written:

$$T_{rot} = \frac{1}{2}(\omega_L)^T I_L\omega_L + \frac{1}{2}(\omega_R)^T I_R\omega_R + \frac{1}{2}(\omega_B)^T I_B\omega_B \tag{7}$$

The inertia matrices are assumed to have a diagonal form, characterized by:

$$I_L = I_R = diag\{K, J, K\} \qquad I_B = diag\{I_1, I_2, I_3\} \tag{8}$$

The potential energy of 2WBMR is given by:

$$V = m_B g l\cos\alpha \tag{9}$$

The Lagrange is defined by:

$$L = T - V = T_{trans} + T_{rot} - V \tag{10}$$

To model the system, the Euler-Lagrange equations are utilized as functions of the following six generalized coordinates:

$$p_1 = x_C, \quad p_2 = y_C, \quad p_3 = \alpha, \quad p_4 = \beta, \quad p_5 = \gamma_L, \quad p_6 = \gamma_R \tag{11}$$

Now the Lagrange equation of motion is given by:

$$\frac{\mathrm{d}}{\mathrm{d}t}\left(\frac{\partial L}{\partial \dot{p}_i}\right)-\frac{\partial L}{\partial p_i}=P_i+\sum_j \lambda_j a_{ji} \qquad (i=1\sim 6, \quad j=1\sim 3) \tag{12}$$

The nonholonomic constraints presented earlier are related to the Lagrange multipliers as follows:

$$\begin{aligned} a_{1i} &= \frac{\partial}{\partial \dot{p}_i}\left(\dot{x}_C\cos\beta+\dot{y}_C\sin\beta-\frac{d}{2}\dot{\beta}-r\dot{\gamma}_L\right), \\ a_{2i} &= \frac{\partial}{\partial \dot{p}_i}\left(\dot{x}_C\cos\beta+\dot{y}_C\sin\beta+\frac{d}{2}\dot{\beta}-r\dot{\gamma}_R\right), \\ a_{3i} &= \frac{\partial}{\partial \dot{p}_i}\left(\dot{x}_C\sin\beta-\dot{y}_C\cos\beta\right). \end{aligned} \tag{13}$$

In this context, each number a_{1i}, a_{2i}, a_{3i} represents a motion constraint of the system based on the nonholonomic equations.

The external forces acting on the system corresponding to the six coordinates can be expressed as:

$$\begin{aligned} &P_1=P_2=P_4=0, \quad P_3=-(P_5+P_6), \\ &P_5=T_L-f_L=T_L-c_f(\dot{\gamma}_L-\dot{\alpha}), \\ &P_6=T_R-f_R=T_R-c_f(\dot{\gamma}_R-\dot{\alpha}). \end{aligned} \tag{14}$$

with c_f as the coefficient of viscous friction on the wheel axis. When applying the Lagrange equations to the six generalized coordinates, six Lagrange equations containing Lagrange multipliers are obtained. After solving these equations without the appearance of Lagrange multipliers, three sets of equations are derived as follows:

$$\begin{aligned} &\left(m_B+2m_W+2\frac{J}{r^2}\right)\ddot{x}-m_Bl\left(\dot{\beta}^2+\dot{\alpha}^2\right)\sin\alpha+m_Bl\cos\alpha\ddot{\alpha} \\ &+\frac{2}{r}c_f\left(\frac{\dot{x}}{r}-\dot{\alpha}\right)=\frac{T_L+T_R}{r} \\ &\left(I_2+m_Bl^2\right)\ddot{\alpha}+m_Bl\cos\alpha\ddot{x}+(I_3-I_1-m_Bl^2)\dot{\beta}^2\sin\alpha\cos\alpha \\ &\quad -2c_f\left(\frac{\dot{x}}{r}-\dot{\alpha}\right)-m_Blg\sin\alpha=-(T_L+T_R) \\ &\left(I_3+2K+m_W\frac{d^2}{2}+J\frac{d^2}{2r^2}-(I_3-I_1-m_Bl^2)\sin^2\alpha\right)\ddot{\beta} \\ &\quad +c_f\dot{\beta}\frac{d^2}{2r^2}+\left(m_Bl\dot{x}-2(I_3-I_1-m_Bl^2)\dot{\alpha}\cos\alpha\right)\dot{\beta}\sin\alpha \\ &=\frac{(T_R-T_L)d}{2r} \end{aligned} \tag{15}$$

The general form of the robot's dynamic equation is:

$$M\ddot{q}+C\dot{q}+D\dot{q}+G=B\tau \tag{16}$$

where M is the inertia matrix, C is the centrifugal and Coriolis force matrix, D is the damping matrix, B is the input matrix, τ is the input variables respectively, and the state $q=\begin{bmatrix} x & \alpha & \beta \end{bmatrix}^T$.

With the output of the model determined by three states, x, α, β, it is necessary to derive the robot's dynamic equation in matrix form from (16). Therefore, after converting to this matrix form, the computed matrices are as follows:

$$\begin{aligned} M &= \begin{bmatrix} a_{11} & a_{12} & 0 \\ a_{21} & a_{22} & 0 \\ 0 & 0 & a_{33} \end{bmatrix}, C = \begin{bmatrix} 0 & c_{12} & c_{13} \\ 0 & 0 & c_{23} \\ c_{31} & c_{32} & c_{33} \end{bmatrix}, \\ G &= \begin{bmatrix} 0 \\ -m_Blg\sin\alpha \\ 0 \end{bmatrix}, B = \begin{bmatrix} 1/r & 1/r \\ -1 & -1 \\ -d/2r & d/2r \end{bmatrix}, \\ D &= \begin{bmatrix} d_{11} & d_{12} & 0 \\ d_{21} & d_{22} & 0 \\ 0 & 0 & d_{33} \end{bmatrix}, \tau = \begin{bmatrix} T_L \\ T_R \end{bmatrix}. \end{aligned} \tag{17}$$

and

$$\begin{aligned} a_{11} &= m_B+2m_W+2J/r^2, \\ a_{12} &= a_{21} = m_Bl\cos\alpha, \\ a_{22} &= m_Bl\cos\alpha, \\ a_{33} &= I_3+2K+m_W\frac{d^2}{2}+J\frac{d^2}{2r^2}-(I_3-I_1-m_Bl^2)\sin^2\alpha, \end{aligned}$$

$$\begin{aligned} c_{31} &= m_Bl\dot{\beta}^2\sin\alpha, \\ c_{12} &= m_Bl\dot{\alpha}\sin\alpha, \\ c_{13} &= m_Bl\dot{\beta}\sin\alpha, \\ c_{23} &= (I_3-I_1-m_Bl^2)\beta\sin\alpha\cos\alpha, \\ c_{32} &= -(I_3-I_1-m_Bl^2)\dot{\beta}\sin\alpha\cos\alpha, \\ c_{33} &= -(I_3-I_1-m_Bl^2)\dot{\alpha}\sin\alpha\cos\alpha, \\ d_{11} &= \frac{2c_\alpha}{r^2}, \\ d_{12} &= d_{21} = -\frac{2c_\alpha}{r}, \\ d_{22} &= 2c_\alpha, \\ d_{33} &= \left(\frac{d^2}{2r^2}\right)c_f. \end{aligned}$$

In the future, The model can be adapted to further develop a two-legged wheeled balancing robot, with the core balance control derived from the current research. This demonstrates adaptability for various types of balancing robots that evolve from 2WBMR and can operate on more complex terrains.

B. Design of HSMC Combined with SMC Controller

To achieve effective stabilization of the 2WBMR system, a controller combining Hierarchical Sliding Mode Control (HSMC) with Sliding Mode Control (SMC) is designed, see Fig. 2. This section details the mathematical formulation and implementation of the combined HSMC-SMC controller, focusing on the control strategy and its application to the 2WBMR system. Initially, it is necessary to determine the mathematical equations of the system. By multiplying both sides of equation

(16) by the inverse of matrix M, the resulting system can be expressed in the following form:

$$\begin{cases} \dot{x}_1 = x_2 \\ \dot{x}_2 = f_1 + g_1 u_1 \\ \dot{x}_3 = x_4 \\ \dot{x}_4 = f_2 + g_2 u_1 \\ \dot{x}_5 = x_6 \\ \dot{x}_6 = f_3 + g_3 u_2 \end{cases} \tag{18}$$

In which X and u represent the state of the system and the input relationship, respectively, taking the form:

$$X = \begin{bmatrix} x_1 & x_2 & x_3 & x_4 & x_5 & x_6 \end{bmatrix}^T = \begin{bmatrix} x & \dot{x} & \alpha & \dot{\alpha} & \beta & \dot{\beta} \end{bmatrix}^T \tag{19}$$

$$u = \begin{bmatrix} u_1 & u_2 \end{bmatrix}^T = \begin{bmatrix} T_L + T_R & T_L - T_R \end{bmatrix}^T \tag{20}$$

1) Hierarchical Sliding Mode Control: To design HSMC, there are four states of the system that need to be controlled, namely position (x), velocity $(\dot{x})$, pitch angles (α) and pitch rate $(\dot{\alpha})$. The errors between these states and the reference are:

$$\begin{cases} e_1 = x - x_d \\ e_2 = \dot{x} - \dot{x}_d \\ e_3 = \alpha - \alpha_d \\ e_4 = \dot{\alpha} - \dot{\alpha}_d \end{cases} \tag{21}$$

Next, the two first-layer sliding surfaces of the system are constructed:

$$\begin{cases} s_1 = c_1 e_1 + e_2 \\ s_2 = c_2 e_3 + e_4 \end{cases} \tag{22}$$

where c_1 and c_2 are positive control parameters. The second-layer sliding surface is synthesized from the combination of the two first-layer sliding surfaces. Specifically, it is defined as:

$$S = \lambda s_1 + \gamma s_2 \tag{23}$$

By setting $\dot{s}_1 = 0$ and using the equation $\dot{x}_2$ from equation 20, the equivalent control law u_{eq1} is obtained as follows:

$$u_{eq1} = -(c_1 \dot{e}_1 + f_1 - \ddot{x}_d)/g_1 \tag{24}$$

Similarly, the second equivalent control law u_{eq2} is derived as:

$$u_{eq2} = -(c_2 \dot{e}_3 + f_2 - \ddot{\alpha}_d)/g_2 \tag{25}$$

To achieve the desired reference, the control input u_1 based on HSMC can be determined as:

$$u_1 = u_{eq1} + u_{eq2} + u_{sw} \tag{26}$$

where u_{sw} is given by:

$$u_{sw} = -(\lambda g_1 u_{eq2} + \gamma g_2 u_{eq1} + \eta_1 sign(S) + k_1 S)/(\lambda g_1 + \gamma g_2) \tag{27}$$

Here, η_1 and k_1 are positive parameters. To demonstrate the stability of the controller, the Lyapunov function is chosen as:

$$V = \frac{1}{2} S^2 \tag{28}$$

The time derivative of the Lyapunov function V is given by:

$$\begin{aligned} \dot{V} &= S\dot{S} \\ &= S(\lambda \dot{s}_1 + \gamma \dot{s}_2) \\ &= S[\lambda(c_1 \dot{e}_1 + \dot{e}_2) + \gamma(c_2 \dot{e}_3 + \dot{e}_4)] \\ &= S\left[\lambda(c_1 \dot{e}_1 + f_1 + g_1 u_1 - \ddot{x}_d) + \gamma(c_2 \dot{e}_3 + f_2 + g_2 u_1 - \ddot{\alpha}_d)\right] \\ &= S\left[\lambda(c_1 \dot{e}_1 + f_1 + g_1(u_{eq1} + u_{eq2} + u_{sw}) - \ddot{x}_d)\right. \\ &\quad \left. + \gamma(c_2 \dot{e}_3 + f_2 + g_2(u_{eq1} + u_{eq2} + u_{sw}) - \ddot{\alpha}_d)\right] \\ &= S\left[\lambda g_1(u_{eq2} + u_{sw}) + \gamma g_2(u_{eq1} + u_{sw})\right] \\ &= S\left[(\lambda g_1 + \gamma g_2) u_{sw} + \lambda g_1 u_{eq2} + \gamma g_2 u_{eq1}\right] \\ &= S(-\eta_1 \mathrm{sign}(S) - k_1 S) \\ &= -\eta_1 |S| - k_1 S^2 \end{aligned} \tag{29}$$

Finally, the result is obtained:

$$\dot{V} = -\eta_1 |S| - k_1 S^2 < 0 \tag{30}$$

From equation (30), it can be inferred that 2WBMR system is stable based on the Lyapunov criterion. At that point, the Lyapunov function measures the system's energy (which is always positive), and its derivative represents how this energy changes. A negative derivative indicates that the Lyapunov energy is approaching zero, meaning the system is moving towards a stable state. That lead to the sliding surface S converging to zero in finite time, which is equivalent to both sliding surfaces s_1 and s_2 converging to zero. Thus, with the positive coefficients c_1 and c_2, as s_1 and s_2 approach 0, the errors will also stabilize and approach 0.

2) Sliding Mode Control: From equation (18), the yaw state is controlled by u_2. Therefore, it is possible to design SMC to stabilize yaw angles (β) and yaw rate $(\dot{\beta})$. The error between the yaw state and yaw reference can be determined as follows:

$$\begin{cases} e_5 = \beta - \beta_d \\ e_6 = \dot{\beta} - \dot{\beta}_d \end{cases} \tag{31}$$

Sliding surface based on SMC is written as:

$$s_3 = c_3 e_5 + e_6 \tag{32}$$

Taking the derivative of this sliding surface, we have:

$$\dot{s}_3 = c_3 \dot{e}_5 + \dot{e}_6 = c_3 \dot{e}_5 + f_3 + g_3 u_2 - \ddot{\beta}_d \tag{33}$$

Select the Lyapunov function:

$$V_3 = \frac{1}{2} s_3^2 \tag{34}$$

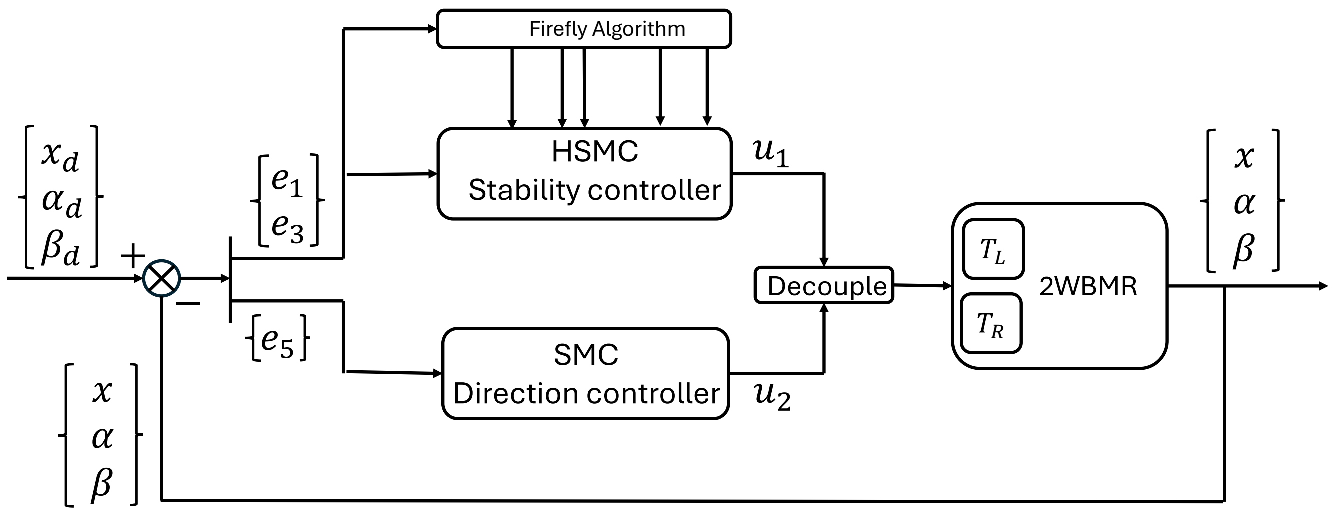

Fig. 2. Control structure

Taking the derivative of both sides of equation (36), we have:

$$\dot{V}_3 = s_3\dot{s}_3 = s_3(c_3\dot{e}_5 + \dot{e}_6) = s_3(c_3\dot{e}_5 + f_3 + g_3u_2 - \ddot{\beta}_d) \quad (35)$$

The goal to be achieved is $\dot{V}_3 < 0$. Therefore, the input control signal u_2 can be selected as follows:

$$u_2 = (1/g_3)(-c_3\dot{e}_5 - f_3 + \ddot{\beta}_d - \eta_2 sign(s_3) - k_2s_3) \quad (36)$$

With η_2 and k_2 being positive constants. By substituting u_2 and $\dot{V}_3$, we can easily prove: $\dot{V}_3 = -\eta_2|s_3| - k_2s_3^2 < 0$ and according Lyapunov criterion, s_3 and e_5 converges to zero. Then yaw state is stable.

C. FA Optimization Algorithm

The Firefly Algorithm (FA) is a nature-inspired optimization technique that mimics the behavior of fireflies, particularly their bioluminescent communication patterns. First introduced by Xin-She Yang, this algorithm is based on the idea that fireflies are attracted to each other based on the intensity of their flashes. In the FA, the brightness of each firefly corresponds to the quality of a potential solution within a multidimensional search space. The brightness is determined by the fitness function specific to the optimization problem.

The algorithm simulates a population of fireflies where each firefly adjusts its position iteratively by being attracted to brighter fireflies. If a firefly finds another firefly that has a brighter intensity, it moves toward that firefly. The distance between fireflies and the light intensity they emit define the movement's magnitude and direction. The process iterates, with fireflies converging towards optimal or near-optimal solutions in the search space, as shown in the algorithm **Algorithm 2**.

The movement of the i-th firefly towards the j-th firefly is modeled as:

$$x_i^{k+1} = x_i^k + \mu_0 e^{-\xi r_{ij}^2}(x_j^k - x_i^k) + \sigma\epsilon_i \quad (37)$$

Where r_{ij} represents the distance between fireflies i and j, μ_0 is the attraction coefficient, ξ is the light absorption coefficient, and $\sigma\epsilon_i$ introduces randomization to diversify the search. The first term allows the firefly to follow the brighter one, while the second term ensures exploration of the search space through random movement. The coefficient ξ controls the firefly's visibility, reducing the attraction between fireflies as the distance increases.Thus, by continuously moving toward the position of brighter and closer fireflies (with the attraction coefficient ξ gradually decreasing) and by reducing the randomness factor σ, the fireflies will converge to an optimal point as they gather in one area, usually around a local optimum solution. In addition to gradually converging towards the global solution, the fireflies continue to move randomly around the region via the randomness factor σ, allowing them to explore new local optima.

Like other optimization techniques, the FA balances exploration and exploitation. During the initial iterations, larger values of the randomization factor σ promote exploration across the search space. As the algorithm proceeds, σ is gradually reduced, enabling fireflies to focus on exploiting areas around the brightest solutions found so far. This balance ensures that the fireflies do not prematurely converge to suboptimal solutions while still refining their search around the most promising areas.In the initial runs, we can accelerate the convergence by reducing the randomness factor σ and increasing the light absorption coefficient ξ so that the fireflies move faster towards brighter points. Conversely, when aiming to improve the optimality of the convergence result, we can increase the randomness factor σ to enhance the fireflies' exploration of the search space and discover new convergence points.

The firefly algorithm's ability to adjust the attraction between fireflies and combine randomness in the search process makes it particularly effective for a variety of optimization problems. Similar to Particle Swarm Optimization (PSO), FA also involves tuning several parameters, such as the light absorption coefficient ξ and the randomization factor σ, to achieve better convergence and prevent being trapped in local optima.In addition, by balancing between optimization and exploration capabilities, we can accelerate the convergence rate through the careful selection of the number of fireflies, the light absorption coefficient ξ, and the randomness factor σ.

In the implementation provided, the *range* defines the boundaries of the search space, while the parameters σ, ξ, and δ control the behavior of the fireflies. The number of generations determines the total iterations, where the swarm dynamically adjusts to find the optimal solution.

Algorithm 2 Firefly Algorithm diagram

```
Input: Number of fireflies n, ranges for variables, parameters σ, ξ, δ.
Output: Best solution found.
Initialize firefly positions xn randomly within the specified ranges.
Calculate initial brightness Lightn.
for each generation T do
    for each firefly i do
        for each best firefly j do
            Calculate distance r between fireflies i and j.
            if Lightn(i) < Lightn(j) then
                Calculate absorption coefficient μ ← μ0 · e^(−γr^2).
                Update position xn(i) ← (1 − μ) · xn(i) + μ · xn(j) + ξ · (rand(1, d) − 0.5).
            end if
        end for
        Limit position xn(i) within the specified range.
    end for
    Evaluate brightness Lightn based on updated positions.
    Update randomness parameter ξ ← ξ · δ.
end for
Record the best solution found.
Display the best solution and running time.
```

III. Results and Discussion

The main results presented in this study include validating the stability of the proposed method, comparing it with the PID control method, and using the Firefly Algorithm (FA) to optimize the parameters of the proposed controller to enhance control quality. The performance of the HSMC controller, in conjunction with the firefly algorithm, is assessed through simulations conducted using Simulink/MATLAB software.

The the parameters of the 2WBMR system are: $d = 0.15(m)$, $l = 0.5(m)$, $r = 0.11(m)$, $m_B = 6.575(kg)$, $m_W = 0.2121(kg)$, $J = 2.651 \times 10^{-4}(kgm^2)$, $K = 5.229 \times 10^{-3}(kgm^2)$, $I_1 = 1.128 \times 10^{-1}(kgm^2)$, $I_2 = 1.248 \times 10^{-1}(kgm^2)$, $I_3 = 4.641 \times 10^{-3}(kgm^2)$, $g = 9.81(m/s^2)$, $c_\alpha = 0.1$.

A. HSMC-SMC

B. Stable Control

In this subsection, to verify the stability of the HSMC-SMC controller, simulations were conducted using Matlab with the following adaptive control parameters: $c_1 = 4, c_2 = 5, k_1 = 2, \lambda = 18, \beta = 8.7, c_3 = 10$, and $k_3 = 10$. The simulation results for the state variables, including the position x, angle α, and angle β, are presented in Fig. 3.

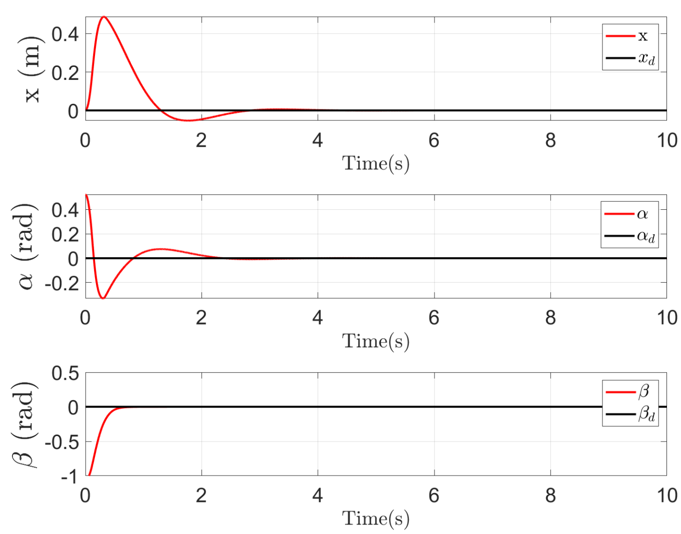

Fig. 3. System response under HSMC - SMC control

From the simulation results with the initial values $\alpha_0 = \frac{\pi}{6}$ and $\beta_0 = -\frac{\pi}{2}$, it is observed that the controller performs well in stabilizing the angle α with minimal overshoot and remains stable within 2 seconds. The settling time of up to nearly 2 seconds is due to the output signal being constrained during the simulation process, ensuring that the output torque is more suitable for real-world applications. The results demonstrate a rapid response and robust stability, making it well-suited for industrial environments with disturbances and complex terrains. In future work, building on the current results, we will focus on tracking control to enable the model to balance and follow a trajectory.

C. Comparision

In this section, to demonstrate the superiority of the proposed method over the previously existing methods, we conducted several comparisons of the stable control results between the proposed HSMC-SMC controller and the stability controller designed using the PID method. The initial conditions are kept the same as $\alpha_0 = \frac{\pi}{6}$ and $\beta_0 = -\frac{\pi}{2}$, and the comparison results are shown in Fig. 4.

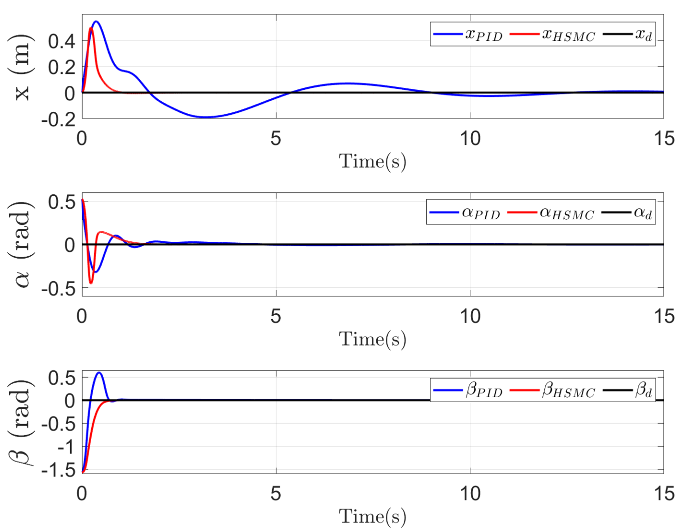

Fig. 4. Comparison results

Based on the comparison results in Fig. 4, it can be observed that the HSMC controller demonstrates significantly superior stability performance compared to the PID controller. Firstly, when comparing the stabilization speed, HSMC shows a much faster response time, especially for the x coordinate, where HSMC achieves stabilization in 1.2 seconds, while PID takes nearly 15 seconds. Regarding overshoot, the HSMC controller also performs much better, as shown in the responses of the angles α and β, particularly the β angle with an overshoot of nearly 30%.

D. Firefly Algorithm

In this subsection, the firefly algorithm is employed to search for and optimize the control parameters of the HSMC controller, specifically the parameters $c_1, c_2, \eta_1, \lambda, \gamma$. The cost function used to evaluate the brightness (efficiency) is defined as follows:

$$F = \frac{1}{1 + IAE_x + IAE_\theta} \tag{38}$$

With IAE_X, IAE_θ is Integral of Absolute Error of coordinates, vertical angles, rotation angles. With the IAE error set in the sample to ensure the smallest error value, the cost function will have the maximum value corresponding to the highest brightness, in order to align with the optimization algorithm to reach the point with the highest brightness. Table II presents the results of the FA algorithm used to tune the control parameters of the HSMC controller and the cost function F shown in Fig. 5.

TABLE II. THE PARAMETERS OF THE CONTROLLER IN DIFFERENT ITERATIONS

Iteration	c_1	c_2	k_1	λ	γ	F
$n = 5$	2.8821	7.8619	29.5338	3.3849	1.7383	0.6777
$n = 10$	1.9633	4.6157	18.5637	7.8249	3.5755	0.7354

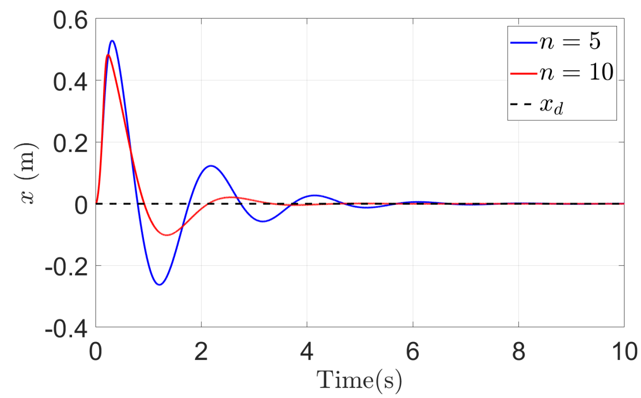

(a) Coordinates x

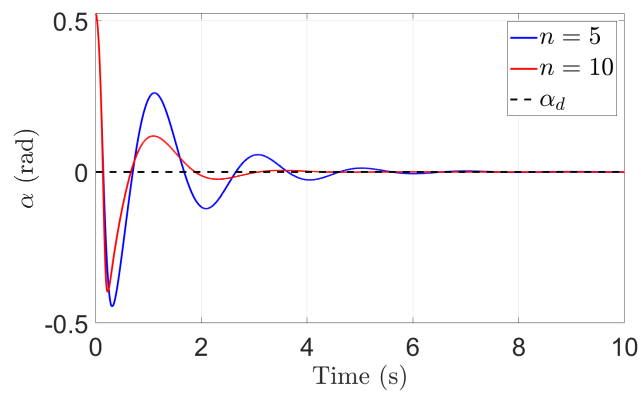

(b) Angle α

Fig. 5. Results demonstrating variations in response to different parameters.

From Fig. 4, we observe that the parameters obtained at the 10th iteration yield a significantly better response in the x-coordinate and the angle α compared to the parameters from the 5th iteration. This indicates that the algorithm successfully achieved its goal of optimizing the control parameters for the HSMC controller.

In addition, A comparative study was conducted to evaluate the optimization performance of the Firefly Algorithm (FA) against the widely used Particle Swarm Optimization (PSO) algorithm. The results, as presented in Table III, indicate that FA demonstrates superior convergence speed and optimization quality, achieving a 10% improvement in the final optimization result compared to PSO. Both algorithms were evaluated under identical conditions, including the number of offspring, iterations, and similar runtime durations (446 seconds for PSO and 534 seconds for FA). The objective function employed for this assessment was:

$$X = IAE_x + IAE_\theta$$

which combines the integral of absolute errors of the system's variables.

TABLE III. COMPARISON OF PSO AND FA BY ITERATION

Iteration	PSO	FA
1	1.441334	0.669196
2	1.075355	0.611261
3	1.044186	0.570133
4	0.517183	0.426512
5	0.517183	0.385446
10	0.405362	0.376905
15	0.405362	0.376388
20	0.405324	0.375243
25	0.396149	0.374891

Thus, through the simulation results with different numbers of loops and the comparison results with the PSO algorithm, it has been proven that the application of the Firefly Algorithm (FA) to optimize control parameters for the HSMC controller is completely feasible and demonstrates superior efficiency compared to current popular optimization methods such as PSO.

IV. CONCLUSION

The present study introduces an integrated control strategy for Two-Wheeled Balancing Mobile Robots (2WBMRs) by combining Hierarchical Sliding Mode Control (HSMC) and Sliding Mode Control (SMC), optimized through the Firefly Algorithm (FA). Our approach addresses key challenges associated with traditional control methods by optimizing control parameters to enhance stability and efficiency. The simulation results demonstrated that the proposed HSMC-SMC controller, optimized by FA, achieved a significant reduction in chattering and improved response times, with the HSMC achieving stabilization in 1.2 seconds compared to nearly 15 seconds for a traditional PID controller. Furthermore, the optimization process reduced chattering amplitude by approximately 30%, demonstrating the effectiveness of our approach in real-time control scenarios.

Our results highlight the practical implications of the proposed control strategy, particularly in industrial automation, autonomous transportation, and mobile robotics, where precise control, stability, and quick adaptation to varying conditions are essential. By improving response times and reducing control oscillations, this approach offers a more robust and reliable solution for complex, nonlinear systems. However, it is important to acknowledge that our study primarily focused on stability in balancing scenarios, and future work will explore extended applications, such as trajectory tracking and enhanced disturbance rejection, which would further validate the real-world applicability of our method.

Despite the promising results, there are certain limitations to our approach. The computational complexity of the optimization process can be influenced by factors such as the system model and computational hardware, and there is a potential risk of the FA getting trapped in local optima, which depends on parameter tuning. Addressing these challenges will be crucial in future research, where we plan to test different optimization algorithms in combination with HSMC and apply our method to more complex robotic systems.

Our findings contribute to the broader field of nonlinear control by providing a comprehensive control strategy that integrates HSMC for system stability and SMC for precise direction control. The use of FA for parameter optimization opens up new possibilities for enhancing control performance across various nonlinear, underactuated systems. This study emphasizes the need for adaptive, efficient control solutions in robotics and highlights how integrated control and optimization can advance existing methods, particularly in environments with dynamic and unpredictable conditions. Future work should continue to explore the full potential of FA and other optimization techniques, including testing in real-world applications to validate the robustness and practical benefits of our approach.

In conclusion, the integration of HSMC, SMC, and the Firefly Algorithm represents a significant step forward in developing advanced control systems that are adaptable, efficient, and capable of handling real-world constraints. We encourage further research to build on these findings, exploring new control strategies and optimization methods that can be applied across various industries, ultimately enhancing the design of control systems for diverse robotic applications.

ACKNOWLEDGMENT

This research was funded by Hanoi University of Science and Technology (HUST) under project number T2023-PC-022.

REFERENCES

[1] N. Jayasekara, B. Kulathunge, H. Premaratne, I. Nilam, S. Rajapaksha, and J. Krishara, "Revolutionizing Accessibility: Smart Wheelchair Robot and Mobile Application for Mobility, Assistance, and Home Management," *Journal of Robotics and Control (JRC)*, vol. 5, no. 1, pp. 27–53, 2023, doi: 10.18196/jrc.v5i1.20057.

[2] M. R. Islam, M. R. T. Hossain, and S. C. Banik, "Synchronizing of Stabilizing Platform Mounted on a Two-Wheeled Robot," *Journal of Robotics and Control (JRC)*, vol. 2, no. 6, 2021, doi: 10.18196/jrc.26136.

[3] C. HY, "Hybrid 5G Positioning Systems with Applications to Mobile Robot Technology," *Advances in Robotic Technology*, vol. 1, no. 1, pp. 1–5, 2023, doi: 10.23880/art-16000106.

[4] L. Yunze, "Analysis of the application of industrial robots in intelligent manufacturing," *International Journal of Frontiers in Engineering Technology*, vol. 4, no. 7, 2022, doi: 10.25236/IJFET.2022.040713.

[5] A. A. Aldhalemi, A. A. Chlaihawi, and A. Al-Ghanimi, "Design and Implementation of a Remotely Controlled Two-Wheel Self-Balancing Robot," *IOP Conference Series: Materials Science and Engineering*, vol. 1067, no. 1, 2021, doi: 10.1088/1757-899x/1067/1/012132.

[6] V.-A. Nguyen, L. Vermeiren, A. Dequidt, A.-T. Nguyen, M. Dambrine, and L. Cung, "Takagi-Sugeno fuzzy descriptor approach for trajectory control of a 2-DOF serial manipulator," *2018 13th IEEE Conference on Industrial Electronics and Applications (ICIEA)*, vol. 6, pp. 1284–1289, 2018, doi: 10.1109/iciea.2018.8397907.

[7] A. T. Nguyen, A. Dequidt, V. A. Nguyen, L. Vermeiren, and M. Dambrine, "Fuzzy descriptor tracking control with guaranteed $L\infty$ error-bound for robot manipulators," *Transactions of the Institute of Measurement and Control*, vol. 43, no. 6, pp. 1404–1415, 2020, doi: 10.1177/0142331220979262.

[8] V. A. Nguyen, A. T. Nguyen, A. Dequidt, L. Vermeiren, and M. Dambrine, "A Robust Descriptor Approach for Nonlinear Tracking Control of Serial Robots," *2018 IEEE Conference on Decision and Control (CDC)*, vol. 8, pp. 6906–6911, 2018, doi: 10.1109/cdc.2018.8619750.

[9] J. Li, H. Qin, J. Wang, and J. Li, "OpenStreetMap-Based Autonomous Navigation for the Four Wheel-Legged Robot Via 3D-Lidar and CCD Camera," *IEEE Transactions on Industrial Electronics*, vol. 69, no. 3, pp. 2708–2717, 2022, doi: 10.1109/tie.2021.3070508.

[10] Y. Xie *et al*., "Coupled fractional-order sliding mode control and obstacle avoidance of a four-wheeled steerable mobile robot," *ISA Transactions*, vol. 108, pp. 282–294, 2021, doi: 10.1016/j.isatra.2020.08.025.

[11] A. Kharola, "Analysing dynamics of two-wheel mobile robot for real-time development of chatbot," *International Journal of Applied Nonlinear Science*, vol. 3, no. 4, 2022, doi: 10.1504/ijans.2022.130490.

[12] H. Mohsin, A. Aldair, and W. Al-Hussaibi, "Robust Control Design for Two-Wheel Self-Balanced Mobile Robot," *Iraqi Journal for Electrical and Electronic Engineering*, vol. 19, no. 1, pp. 38–46, 2022, doi: 10.37917/ijeee.19.1.5.

[13] C. Yan and X. Li, "Research on Stability Control System of Two-Wheel Heavy-Load Self-Balancing Vehicles in Complex Terrain," *Applied Sciences*, vol. 14, no. 17, 2024, doi: 10.3390/app14177682.

[14] T. Yasui, M. Sasaki, K. Matsushita, J. Muguro, W. Njeri, and T. Mulembo, "Equilibrium Control of Robot Arm Tip Mounted on a Transfer Coaxial Two-Wheel Robot," *Jurnal Nasional Teknik Elektro*, 2023, doi: 10.25077/jnte.v12n2.1106.2023.

[15] T. Van Nguyen, H. X. Le, H. V. Tran, D. A. Nguyen, M. N. Nguyen and L. Nguyen, "Adaptive Dynamic Programming based Control Scheme for Uncertain Two-Wheel Robots," *2021 IEEE International Conference on Autonomous Robot Systems and Competitions (ICARSC)*, pp. 111-116, 2021, doi: 10.1109/ICARSC52212.2021.9429805.

[16] H. Yanying, L. Yezhuo, W. Jianxu, L. Xingjie, and Y. Yanan, "Design and Mobility Analysis of a Multi-mode Two-wheel Mobile Robot," *Journal of Mechanical Engineering*, vol. 55, no. 23, pp. 83–92, 2019, doi: 10.3901/jme.2019.23.083.

[17] N. C. Cuong and H. D. Co, "Balancing and Trajectory Tracking Control for Two-Wheeled Self-Balancing Robot," *International Journal of Engineering Trends and Technology*, vol. 72, no. 7, pp. 45–57, 2024, doi: 10.14445/22315381/ijett-v72i7p105.

[18] R. Tsutada, T.-T. Hoang, and C.-K. Pham, "An Obstacle Avoidance Two-Wheeled Self-Balancing Robot," *International Journal of Mechanical Engineering and Robotics Research*, pp. 1–7, 2022, doi: 10.18178/ijmerr.11.1.1-7.

[19] Santoso, I. Aula Wardah, P. Slamet, A. Heri Andriawan, and A. Rahman Algopiki, "Design and Build Two Wheel Balancing Robot Simulation with Fuzzy PID," *Proceedings of the 4th International Conference on Advanced Engineering and Technology*, vol. 1, pp. 124–128, 2023, doi: 10.5220/0012108300003680.

[20] J. -X. Chen, N. He and L. He, "Adaptive Double Fuzzy Anti-Integral Saturation PID Control for Self-balancing Robot with Reaction Wheel," *2022 IEEE 17th International Conference on Control & Automation (ICCA)*, pp. 56-61, 2022, doi: 10.1109/ICCA54724.2022.9831956.

[21] S. Malpani, S. Gupta, S. Agarwal, Mohd. Alam, and G. Raj, "Reviewing the Pid Based Technologies Behind Two Wheel Balancing Robot," *International Journal of Technical Research & Science*, pp. 56–60, 2021, doi: 10.30780/specialissue-icaaset021/011.

[22] D. T. Tran, N. M. Hoang, N. H. Loc, Q. T. Truong, and N. T. Nha, "A Fuzzy LQR PID Control for a Two-Legged Wheel Robot with Uncertainties and Variant Height," *Journal of Robotics and Control (JRC)*, vol. 4, no. 5, pp. 612–620, 2023, doi: 10.18196/jrc.v4i5.19448.

[23] X. Feng, S. Liu, Q. Yuan, J. Xiao, and D. Zhao, "Research on wheel-legged robot based on LQR and ADRC," *Scientific Reports*, vol. 13, no. 1, 2023, doi: 10.1038/s41598-023-41462-1.

[24] N. H. Nam, "Control of Two-Wheeled Inverted Pendulum Robot Using Robust Pi and Lqr Controllers," *Journal of Military Science and Technology*, no. 66A, pp. 1–15, 2020, doi: 10.54939/1859-1043.j.mst.66a.2020.1-15.

[25] Ö. ÖZDEMİR and İ. YAZICI, "Real Time Performance Comparison of Buck Converter Circuit Controlled By Discrete Time PID, LQR and SMC Controllers in Continuous-Current Mode," *Sakarya University Journal of Science*, vol. 23, no. 6, pp. 1198–1206, 2019, doi: 10.16984/saufenbilder.467592.

[26] H. E. Ceyhun and A. Goren, "LQR ve Lyapunov temelli iki kontrolcünün kinematik bisiklet tipi model için güzergah izleme performansı karşılaştırması," *Uluslararası Teknolojik Bilimler Dergisi*, vol. 14, no. 3, pp. 153–162, 2022, doi: 10.55974/utbd.1130198.

[27] Y. Karabacak, A. Yasar, and I. Saritas, "Doğrusal Olmayan Manyetik Levitasyon Sisteminin Kontrolü için PID ve LQR Kontrolcülerinin Performans Karşılaştırılması," *Dokuz Eylul University Faculty of Engineering Journal of Science and Engineering*, vol. 25, no. 74, pp. 339–350, 2023, doi: 10.21205/deufmd.2023257407.

[28] M. Okasha, J. Kralev, and M. Islam, "Design and Experimental Comparison of PID, LQR and MPC Stabilizing Controllers for Parrot Mambo Mini-Drone," *Aerospace*, vol. 9, no. 6, 2022, doi: 10.3390/aerospace9060298.

[29] A. Lima-Perez *et al*., "Robust Control of a Two-Wheeled Self-Balancing Mobile Robot," *2021 International Conference on Mechatronics, Electronics and Automotive Engineering (ICMEAE)*, pp. 196–201, 2021, doi: 10.1109/icmeae55138.2021.00038.

[30] X. Wang, D. Wang, M. Du, K. Song, Y. Ni, and Y. Li, "A Two-Layer Trajectory Tracking Control Scheme of Manipulator Based on ELM-SMC for Autonomous Robotic Vehicle," *IEEE Transactions on Automation Science and Engineering*, vol. 21, no. 3, pp. 2337–2348, 2024, doi: 10.1109/tase.2023.3238349.

[31] D. C. Vu, M. D. Pham, T. T. H. Nguyen, T. V. A. Nguyen, and T. L. Nguyen, "Time-optimal trajectory generation and observer-based hierarchical sliding mode control for ballbots with system constraints," *International Journal of Robust and Nonlinear Control*, vol. 34, no. 11, pp. 7580–7610, 2024, doi: 10.1002/rnc.7358.

[32] D. B. Pham, Q. T. Dao, and T. V. A. Nguyen, "Optimized Hierarchical Sliding Mode Control for the Swing-Up and Stabilization of a Rotary Inverted Pendulum," *Automation*, vol. 5, no. 3, pp. 282–296, 2024, doi: 10.3390/automation5030017.

[33] Y. Wei, H. Wang, and Y. Tian, "Adaptive sliding mode observer–based integral sliding mode model-free torque control for elastomer series elastic actuator–based manipulator," *Proceedings of the Institution of Mechanical Engineers, Part I: Journal of Systems and Control Engineering*, vol. 236, no. 5, pp. 1010–1028, 2021, doi: 10.1177/09596518211064757.

[34] M. D. Duong, D. L. Nguyen, T. L. Tong, and Q. T. Dao, "Fast Terminal Sliding-Mode Control with High-Gain Observer for Series Elastic Actuator Robot," *2023 12th International Conference on Control, Automation and Information Sciences (ICCAIS)*, vol. 4, pp. 501–506, 2023, doi: 10.1109/iccais59597.2023.10382384.

[35] V. V. Dinh, M. C. Trinh, T. D. Bui, M. D. Duong, and Q. T. Dao, "Neural network based patient recovery estimation of a PAM-based rehabilitation robot," *Acta Polytechnica*, vol. 63, no. 3, 2023, doi: 10.14311/ap.2023.63.0179.

[36] S. J. Abbas, S. S. Husain, S. Al-Wais, and A. J. Humaidi, "Adaptive Integral Sliding Mode Controller (SMC) Design for Vehicle Steer-by-Wire System," *SAE International Journal of Vehicle Dynamics, Stability, and NVH*, vol. 8, no. 3, 2024, doi: 10.4271/10-08-03-0021

[37] S. M. Amrr and A. Alturki, "Robust Control Design for an Active Magnetic Bearing System Using Advanced Adaptive SMC Technique," *IEEE Access*, vol. 9, pp. 155662–155672, 2021, doi: 10.1109/access.2021.3129140.

[38] H. V. Doan and N. T.-T. Vu, "Adaptive sliding mode control for uncertain wheel mobile robot," *International Journal of Electrical and Computer Engineering (IJECE)*, vol. 13, no. 4, 2023, doi: 10.11591/ijece.v13i4.pp3939-3947.

[39] L. Chen *et al*., "Robust control of reaction wheel bicycle robot via adaptive integral terminal sliding mode," *Nonlinear Dynamics*, vol. 104, no. 3, pp. 2291–2302, 2021, doi: 10.1007/s11071-021-06380-9.

[40] L. Chen *et al*., "Correction to: Robust control of reaction wheel bicycle robot via adaptive integral terminal sliding mode," *Nonlinear Dynamics*, vol. 104, no. 4, pp. 4753–4753, 2021, doi: 10.1007/s11071-021-06473-5.

[41] X. Yu, Y. Feng, and Z. Man, "Terminal Sliding Mode Control – An Overview," *IEEE Open Journal of the Industrial Electronics Society*, vol. 2, pp. 36–52, 2021, doi: 10.1109/ojies.2020.3040412.

[42] L. Chen *et al*., "Robust hierarchical sliding mode control of a two-wheeled self-balancing vehicle using perturbation estimation," *Mechanical Systems and Signal Processing*, vol. 139, 2020, doi: 10.1016/j.ymssp.2019.106584.

[43] C. E. M. Ochoa *et al*., "Active Disturbance Rejection Control for Robot Manipulator," *Journal of Robotics and Control (JRC)*, vol. 3, no. 5, pp. 622–632, 2022, doi: 10.18196/jrc.v3i5.14791.

[44] N. A. Alawad, A. J. Humaidi, and A. S. Alaraji, "Observer Sliding Mode Control Design for lower Exoskeleton system: Rehabilitation Case," *Journal of Robotics and Control (JRC)*, vol. 3, no. 4, pp. 476–482, 2022, doi: 10.18196/jrc.v3i4.15239.

[45] G. A. M. Hernandez, J. D. Téllez, J. E. Carreon, and R. S. G. Ramírez, "ADRC Attitude Controller Based on ROS for a Two-Wheeled Self-Balancing Mobile Robot," *IEEE Access*, vol. 11, pp. 94636–94646, 2023, doi: 10.1109/access.2023.3308948.

[46] W. Xu, "Comparison of anti-interference ability between PID controller and ADRC controller in UAV operation at ocean," *Theoretical and Natural Science*, vol. 5, no. 1, pp. 720–726, 2023, doi: 10.54254/2753-8818/5/20230479.

[47] M. A. Abdalla, G. Yang, and C. Huang, "Performance Comparison of Load Frequency Control for Power System by ADRC Approach and PID Controller," *Journal of Physics: Conference Series*, vol. 1510, no. 1, 2020, doi: 10.1088/1742-6596/1510/1/012007.

[48] G. Gembalczyk, P. Gierlak, and S. Duda, "Control System Design of an Underactuated Dynamic Body Weight Support System Using Its Stability," *Sensors*, vol. 21, no. 15, 2021, doi: 10.3390/s21155051.

[49] W. Guo and D. Liu, "Sliding Mode Observe and Control for the Underactuated Inertia Wheel Pendulum System," *IEEE Access*, vol. 7, pp. 86394–86402, 2019, doi: 10.1109/access.2019.2926082.

[50] X. Liu, P. Hu, and Y. Chen, "Adaptive Hierarchical Sliding Mode Control Based on Extended State Observer for Underactuated Robotic System," *International Journal of Control, Automation and Systems*, vol. 22, no. 3, pp. 1036–1049, 2024, doi: 10.1007/s12555-022-0357-4.

[51] V. T. Nguyen, H. B. Giap, S. F. Su, M. Van, D. V. La, and T. L. Bui, "Design and Experiment of Interval Type-2 Fuzzy Hierarchical Sliding-Mode Control for Pendubot With Uncertainties," *IEEE/ASME Transactions on Mechatronics*, pp. 1–12, 2024, doi: 10.1109/tmech.2024.3457015.

[52] M. Zhang, Y. Zhang, B. Ji, C. Ma, and X. Cheng, "Modeling and energy-based sway reduction control for tower crane systems with double-pendulum and spherical-pendulum effects," *Measurement and Control*, vol. 53, no. 1–2, pp. 141–150, 2019, doi: 10.1177/0020294019877492.

[53] Q. Wu, X. Wang, L. Hua, and M. Xia, "Dynamic analysis and time optimal anti-swing control of double pendulum bridge crane with distributed mass beams," *Mechanical Systems and Signal Processing*, vol. 144, 2020, doi: 10.1016/j.ymssp.2020.106968.

[54] S. Kim and S. Kwon, "Robust transition control of underactuated two-wheeled self-balancing vehicle with semi-online dynamic trajectory planning," *Mechatronics*, vol. 68, 2020, doi: 10.1016/j.mechatronics.2020.102366.

[55] Z. Mai, "Performance comparison between LQR and PID controllers for two-wheeled self-balancing vehicle," *Applied and Computational Engineering*, vol. 9, no. 1, pp. 303–311, 2023, doi: 10.54254/2755-2721/9/20230116.

[56] J. Huo, R. Lin, and M. Yang, "Design and validation of a novel adaptive motion control for a pendulum spherical robot," *Robotica*, vol. 41, no. 7, pp. 2031–2049, 2023, doi: 10.1017/s0263574723000280.

[57] Y. Liu *et al*., "Direction and Trajectory Tracking Control for Nonholonomic Spherical Robot by Combining Sliding Mode Controller and Model Prediction Controller," *IEEE Robotics and Automation Letters*, vol. 7, no. 4, pp. 11617–11624, 2022, doi: 10.1109/lra.2022.3203224.

[58] K. Adamiak, "Chattering-Free Reference Sliding Variable-Based SMC," *Mathematical Problems in Engineering*, vol. 2020, pp. 1–16, 2020, doi: 10.1155/2020/3454090.

[59] S. Ahmad, A. A. Uppal, M. R. Azam, and J. Iqbal, "Chattering Free Sliding Mode Control and State Dependent Kalman Filter Design for Underground Gasification Energy Conversion Process," *Electronics*, vol. 12, no. 4, 2023, doi: 10.3390/electronics12040876.

[60] M. A. Sepestanaki, M. H. Barhaghtalab, S. Mobayen, A. Jalilvand, A. Fekih, and P. Skruch, "Chattering-Free Terminal Sliding Mode Control Based on Adaptive Barrier Function for Chaotic Systems With Unknown Uncertainties," *IEEE Access*, vol. 10, pp. 103469–103484, 2022, doi: 10.1109/access.2022.3209993.

[61] N. Rokbani, B. Neji, M. Slim, S. Mirjalili, and R. Ghandour, "A Multi-Objective Modified PSO for Inverse Kinematics of a 5-DOF Robotic Arm," *Applied Sciences*, vol. 12, no. 14, 2022, doi: 10.3390/app12147091.

[62] S. Kumar, A. Gupta, and R. K. Bindal, "Load-frequency and voltage control for power quality enhancement in a SPV/Wind utility-tied system using GA ; PSO optimization," *Results in Control and Optimization*, vol. 16, 2024, doi: 10.1016/j.rico.2024.100442.

[63] H. Liang, J. Zou, K. Zuo, and M. J. Khan, "An improved genetic algorithm optimization fuzzy controller applied to the wellhead back pressure control system," *Mechanical Systems and Signal Processing*, vol. 142, 2020, doi: 10.1016/j.ymssp.2020.106708.

[64] G. Yüksek, A. N. Mete, and A. Alkaya, "LQR and GA based PID Parameter Optimization: Liquid Level Control Application," *Politeknik Dergisi*, vol. 23, no. 4, pp. 1111–1119, 2020, doi: 10.2339/politeknik.603344.

[65] W. Rahmaniar and A. E. Rakhmania, "Mobile Robot Path Planning in a Trajectory with Multiple Obstacles Using Genetic Algorithms," *Journal of Robotics and Control (JRC)*, vol. 3, no. 3, pp. 1–7, 2021, doi: 10.18196/jrc.v3i1.11024.

[66] R. S.Patil, S. P. Jadhav, M. D. Patil, "Review of Intelligent and Nature-Inspired Algorithms-Based Methods for Tuning PID Controllers in Industrial Applications," *Journal of Robotics and Control (JRC)*, vol. 5, no. 2, pp. 336-358, 2024, doi: https://doi.org/10.18196/jrc.v5i2.20850.

[67] N. Khanduja, B. Bhushan, and S. Mishra, "Control of CSTR using firefly and hybrid firefly-biogeography based optimization (BBFFO) algorithm," *Journal of Information and Optimization Sciences*, vol. 41, no. 6, pp. 1443–1452, 2020, doi: 10.1080/02522667.2020.1809098.

[68] R. Rajeswari and R. S. P. Priya, "Detection With Firefly Algorithm (FA) Based Feature Selection Forautism Spectrum Disorder (ASD) and Machine Learning Classification," *International Journal of Computer Sciences and Engineering*, vol. 7, no. 5, pp. 992–998, 2019, doi: 10.26438/ijcse/v7i5.992998.

[69] M. A. Mohamad and H. Haron, "Hybrid Firefly Algorithm with Artificial Neural Network (FA-ANN) Classification Model for Handwritten Character Recognition," *IOP Conference Series: Materials Science and Engineering*, vol. 864, no. 1, 2020, doi: 10.1088/1757-899x/864/1/012088.

[70] M. Achouri and Y. Zennir, "Path planning and tracking of wheeled mobile robot: using firefly algorithm and kinematic controller combined with sliding mode control," *Journal of the Brazilian Society of Mechanical Sciences and Engineering*, vol. 46, no. 4, 2024, doi: 10.1007/s40430-024-04772-7.

[71] I. A. Hassan, I. A. Abed, and W. A. Al-Hussaibi, "Path Planning and Trajectory Tracking Control for Two-Wheel Mobile Robot," *Journal of Robotics and Control (JRC)*, vol. 5, no. 1, pp. 1–15, 2024, doi: 10.18196/jrc.v5i1.20489.

[72] N. H. Singh, A. Laishram, and K. Thongam, "Optimal Path Planning for Mobile Robot Navigation Using FA-TPM in Cluttered Dynamic Environments," *Procedia Computer Science*, vol. 218, pp. 612–620, 2023, doi: 10.1016/j.procs.2023.01.043.

[73] N. A. K. Zghair and A. S. A. Araji, "Intelligent Hybrid Path Planning Algorithms for Autonomous Mobile Robots," *International Journal of Intelligent Engineering and Systems*, vol. 15, no. 5, pp. 309–325, 2022, doi: 10.22266/ijies2022.1031.28.

[74] R. Raj and B. M. Mohan, "Analytical Structures of Takagi-Sugeno Fuzzy Two-Input Two-Output Proportional-Integral/Proportional-Derivative Controllers With Multiple Fuzzy Sets," *Journal of Dynamic Systems, Measurement, and Control*, vol. 141, no. 5, 2019, doi: 10.1115/1.4042463.

[75] M. H. Ab Talib *et al*., “Experimental evaluation of ride comfort performance for suspension system using PID and fuzzy logic controllers by advanced firefly algorithm,” *Journal of the Brazilian Society of Mechanical Sciences and Engineering*, vol. 45, no. 3, 2023, doi: 10.1007/s40430-023-04057-5.

[76] F. Z. Baghli, Y. Lakhal, and Y. A. E. Kadi, “The Efficiency of an Optimized PID Controller Based on Ant Colony Algorithm (ACO-PID) for the Position Control of a Multi-articulated System,” *Journal of Robotics and Control (JRC)*, vol. 4, no. 3, pp. 289–298, 2023, doi: 10.18196/jrc.v4i3.17709.

[77] R. Kristiyono and W. Wiyono, “Autotuning Fuzzy PID Controller for Speed Control of BLDC Motor,” *Journal of Robotics and Control (JRC)*, vol. 2, no. 5, pp. 400–407, 2021, doi: 10.18196/jrc.25114.

[78] M. Doğan and Ü. Önen, “Trajectory Tracking Control of a Two Wheeled Self-Balancing Robot by Using Sliding Mode Control,” *Konya Journal of Engineering Sciences*, vol. 12, no. 3, pp. 652–670, 2024, doi: 10.36306/konjes.1425949.

[79] S. Yang, H. Pang, L. Liu, L. Zheng, L. Wang, and M. Liu, “A RISE-based asymptotic prescribed performance trajectory tracking control of two-wheeled self-balancing mobile robot,” *Nonlinear Dynamics*, vol. 112, no. 17, pp. 15327–15348, 2024, doi: 10.1007/s11071-024-09569-w.

[80] N. Uddin, “Adaptive Trajectory Tracking Control System of Two-Wheeled Robot,” *Journal of Physics: Conference Series*, vol. 1373, no. 1, 2019, doi: 10.1088/1742-6596/1373/1/012052.